Research Article

Impact of SnF₂ Addition on the Chemical and Electronic Surface Structure of CsSnBr₃

Claudia Hartmann, Satyajit Gupta, Tatyana Bendikov, Xeniya Kozina, Thomas Kunze, Roberto Félix, Gary Hodes,* Regan G. Wilks, David Cahen,* and Marcus Bär*

Read Online

ACCESS | Metrics & More | Article Recommendations | Supporting Information

ABSTRACT: We report on the chemical and electronic structure of cesium tin bromide (CsSnBr₃) and how it is impacted by the addition of 20 mol % tin fluoride (SnF₂) to the precursor solution, using both surface-sensitive lab-based soft X-ray photoelectron spectroscopy (XPS) and near-surface bulk-sensitive synchrotron-based hard XPS (HAXPES). To determine the reproducibility and reliability of conclusions, several (nominally identically prepared) sample sets were investigated. The effects of deposition reproducibility, handling, and transport are found to cause significant changes in the measured properties of the films. Variations in the HAXPES-derived compositions between individual sample sets were observed, but in general, they confirm that the addition of 20 mol % SnF₂ improves coverage of the titanium dioxide substrate by CsSnBr₃ and decreases the oxidation of Sn^II to Sn^IV while also suppressing formation of secondary Br and Cs species. Furthermore, the (surface) composition is found to be Cs-deficient and Sn-rich compared to the nominal stoichiometry. The valence band (VB) shows a SnF₂-induced redistribution of Sn 5s-derived density of states, reflecting the changing Sn^II/Sn^IV ratio. Notwithstanding some variability in the data, we conclude that SnF₂ addition decreases the energy difference between the VB maximum of CsSnBr₃ and the Fermi level, which we explain by defect chemistry considerations.

KEYWORDS: *perovskites, CsSnBr₃, impact of SnF₂, chemical composition, photoemission, thin-film solar cells*
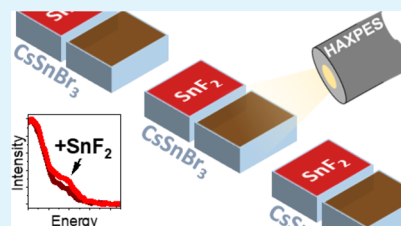
1. INTRODUCTION

Lead-based halide APbX₃ perovskite (HaP) solar cells [with A = methyl ammonium (MA), formamidinium (FA) and/or cesium (Cs⁺), and X = I⁻, Br⁻, and/or Cl⁻] have shown a rapid increase in power conversion efficiencies (PCEs) over the past years, reaching efficiencies beyond 25%.[1−4] Yet, the toxicity of Pb and water-soluble Pb salts (PbX₂) that are products of degradation of HaPs raises environmental concerns, which might restrict the commercialization of Pb-based HaP cells. Therefore, special attention is currently paid to replace Pb with alternative less-toxic elements[5] such as tin,[6,7] germanium,[8] or a combination of bismuth and silver,[9−11] aiming for Pb-free HaPs.

In this paper, we consider Sn-based HaPs (in particular, CsSnBr₃). Although much less studied than Pb-containing HaPs, there is a significant body of work on these Sn-based materials and cells, some of which have been reviewed recently.[12,13] The optical band gap energies of Sn-based HaPs are lower than those of their Pb-containing counterparts (e.g., MASnI₃ has a band gap of ∼1.3 eV compared to ∼1.6 eV for MAPbI₃[14]) and are thus often closer to the optimal range for single-junction photovoltaic cells, calculated within the Shockley−Queisser model.[15] However, so far the highest reported efficiency for these cells is 9.6%,[16] which is more than 2.5 times lower than the best reported efficiencies for Pb-containing devices. Adding SnF₂ to the precursor solution of

Sn-based HaPs enhances the device performance.[12] The underlying mechanism for the SnF₂-induced efficiency gain is, however, still not well understood. Thus, we aim at identifying the effect of adding SnF₂ to the precursor solution on the chemical and electronic structure of the resulting CsSnBr₃ thin-film solar cell absorbers, which are promising candidates for top cells in tandem devices. We find a beneficial effect of the addition of SnF₂ on the ability of CsSnBr₃ to cover the substrate. We identify Sn^IV-type tin and secondary Cs- and Br-derived species to be present in the studied CsSnBr₃ films and that their contribution decreases with addition of SnF₂. Furthermore, an overall enrichment in tin and deficiency of cesium in the surface region are revealed, and high-resolution valence band (VB) spectra show a SnF₂-induced redistribution of Sn 5s-derived density of states (DOS), reflecting the changing Sn^II/Sn^IV ratio.

As deposition and spectroscopic characterization are mainly performed in different laboratories on sample sets that have been similarly prepared, part of the work was also carried out

to study the reproducibility (e.g., of sample preparation) as well as the impact of environmental (e.g., during transport) and handling (after sample preparation and before characterization) factors on the measured data.

2. RESULTS AND DISCUSSION

The impact of adding 20 mol % SnF_2 to the precursor solution on the chemical and electronic structure of the resulting Sn-based HaP was studied by lab-based soft [X-ray photoelectron spectroscopy (XPS)] and synchrotron-based hard (HAXPES) XPS. XPS measurements were performed at the Weizmann Institute of Science (WIS) and at the Helmholtz-Zentrum Berlin für Materialien und Energie GmbH (HZB); all HAXPES measurements were carried out at the HiKE endstation located at HZB's BESSY II KMC-1 beamline.[17,18] All results are obtained on $CsSnBr_3$ films made by the same method as described in ref 19. In previous publications,[19,20] using 20−30 mol % SnF_2 as an additive resulted in the best performing solar cells (best PCE reaching 2.5%).

Two types of samples, $CsSnBr_3$/compact TiO_2/FTO/glass (hereafter referred to as set A) and $CsSnBr_3$ + 20 mol % SnF_2/compact TiO_2/FTO/glass (hereafter referred to as set B), were studied. To study (and account for) any effects related to the reproducibility of sample preparation or handling and the stability of the films during transport from WIS to HZB, in total, five batches of two samples each (sets A_n, B_n, $n = 1-5$) were characterized by XPS at HZB and WIS and by HAXPES at HZB over the course of 4 months. Out of these five batches, two sets produced inconsistent results; neither A_2 nor B_2 had a detectable F 1s signal, which would have been expected for sample B_2. Both samples A_4 and B_4 had a measureable F 1s signal, which was supposed to be absent for A_4 (and attributed to cross-contamination during sample transport). Therefore, sample sets 2 and 4 were excluded from further detailed analysis, as they were not suitable for correlating our spectroscopic results with the addition of SnF_2 to the precursor solution. The remaining sample sets $A_{1,3,5}$ and $B_{1,3,5}$ show clear spectral differences in the HAXPES data (see Figure 1 and the

Supporting Information, Figure S1). In the following, the photoemission (and here mainly the HAXPES) data of A_3 and B_3 are shown as examples and discussed; sample B_3 had the highest fluorine concentration of the remaining samples and, therefore, gives the largest contrast between the $CsSnBr_3$ sample that was prepared with and without 20 mol % SnF_2 being added to the precursor solution (see Figure S2). Note that all HAXPES measurements are used in quantification and mostly mean values are considered when discussing the data and drawing conclusions. Because of the higher surface sensitivity of the XPS data [e.g., the inelastic mean free path (IMFP) of Cs 3d photoelectrons excited with Al Kα (1486.58 eV) and a kinetic energy of 762.58 eV is approximately 2 nm[21] compared to the HAXPES measurements (e.g., the IMFP of Cs 4d photoelectrons excited with 2 keV and a kinetic energy of 1927.6 eV is approximately 4 nm[21]), the latter will be significantly less affected by surface effects (e.g., contamination and/or oxidation), and thus, we will mainly use the HAXPES data for discussion. However, in order to compare the impact of the duration between sample deposition and characterization and/or the impact of transport, we will also use and refer to the measured XPS data.

Figure 1 shows the shallow core levels of the $CsSnBr_3$/compact TiO_2 samples for which no (sample A_3, "$CsSnBr_3$") and 20 mol % SnF_2 (sample B_3, "$CsSnBr_3$ + 20 mol % SnF_2") was added to the precursor solution. All expected core levels originating from $CsSnBr_3$ (i.e., Cs 4d, Cs 5p, Br 3d, and Sn 4d) and, for sample A_3, also lines attributed to the compact TiO_2 substrate (i.e., Ti 3s, Ti 3p, and O 2s) can be identified in the spectra. In contrast to sample A_3, no substrate-related lines can be observed in the spectrum of sample B_3 ($CsSnBr_3$ + 20 mol % SnF_2), suggesting that the SnF_2 additive increases the absorber coverage of the compact TiO_2 substrate, which is further supported by scanning electron microcopy top view images on a similar prepared sample set complementing the HAXPES data (see Figure S3 in the Supporting Information). This improvement of coverage and morphology has also been observed by Koh et al., describing an improved surface coverage of the mesoporous TiO_2 substrate by $FASnI_3$, manifested as a reduced number of pinholes and voids compared to the pure halide perovskite film.[22] Similar observations were made by Liao et al.[23] for $CsSnI_3$ prepared with SnF_2: a larger crystallite size was observed compared to that prepared without SnF_2.[24] Furthermore, a similar reduction of the density of pinholes was found for a low-dimensional form of FA−Sn−I.[25] A systematic study of the $CsSnI_3$ morphology by Marshall et al.[26] showed that actually the excess of Sn (mostly independent of the used anions: F, Cl, Br, and I) is responsible for the improved coverage. While each SnX_2 salt gave a somewhat different morphology, SnF_2 led to the best coverage and smoothest films.[26]

The peak shapes of the Sn 4d, Br 3d, and Cs 4d lines vary between the spectra of A_3 and B_3, indicating the presence of multiple chemical species, which is confirmed by curve fit analysis and discussed in detail below [the complete fit results and more details can be found in the Supporting Information (Figures S4−S6, including related discussion and Experimental Section)].

Figure 2 shows the Sn 4d spectra (along with the O 2s and Cs 5s lines) of samples A_3 and B_3, including curve fit results. For the Sn 4d signal, satisfactory fits of the spectra can be obtained by using two peak doublets, indicating the presence of (at least) two distinct Sn species in both samples. Note that
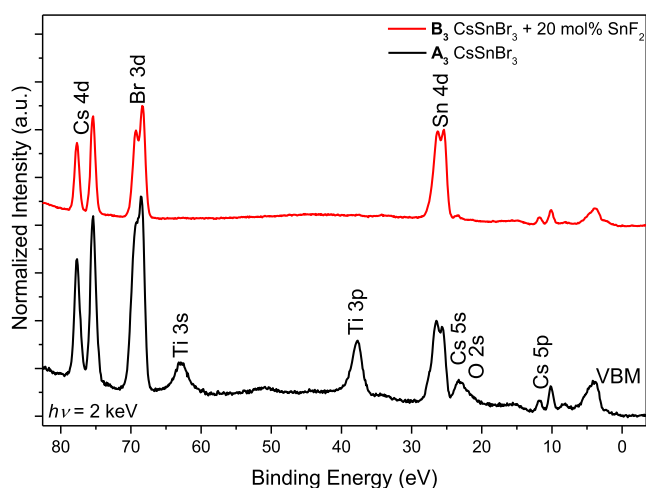

Figure 1. HAXPES spectra of the shallow core-level energy region of $CsSnBr_3$ prepared without (sample A_3, "$CsSnBr_3$", black line) and with 20 mol % SnF_2 (sample B_3, "$CsSnBr_3$ + 20 mol % SnF_2", red line) in the precursor solution. Spectra are shown after background subtraction and normalization to the Sn 4d peak height; vertical offset is added for clarity.
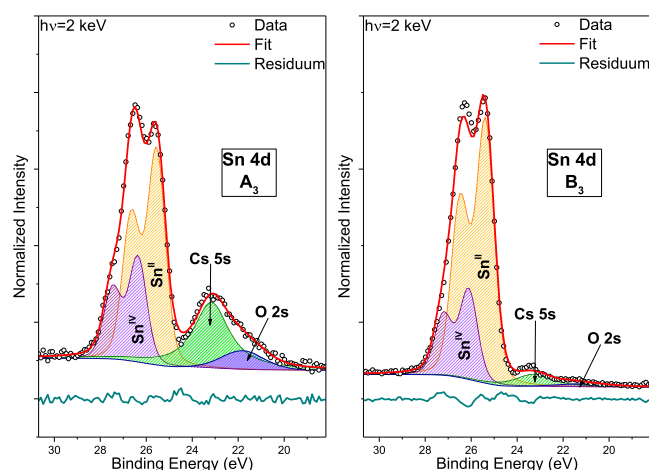
Figure 2. HAXPES detail spectra of the Sn 4d, Cs 5s, and O 2s BE region of $CsSnBr_3$ (A_3, left panel) and $CsSnBr_3$ + 20 mol % SnF_2 (B_3, right panel), shown with curve fit results. The spectra were normalized by the background intensity at BEs around the Fermi level (E_F).

$CsSnBr_3$ samples have been reported to be sensitive to X-rays, but no evidence is found for a (hard) X-ray induced formation of metallic Sn—as previously reported in ref 19 for lab-based XPS measurements—in our HAXPES data. If metallic Sn (Sn^0) were present, the Sn 4d component would be located in approximately the same energy region as the O 2s/Cs 5s peaks, and, because there is no indication of Sn^0 signal in the Sn 3d HAXPES spectra of the same samples (see Figure S8, left panels), this can be excluded. However, accompanying XPS measurements of a $CsSnBr_3$/compact TiO_2/FTO/glass sample (sample A_{WIS}) at WIS do show a metallic Sn contribution to the Sn 3d core level, which is not seen when SnF_2 is added to the precursor solution [see the Sn 3d spectrum of a $CsSnBr_3$ + 20 mol % SnF_2/compact TiO_2/FTO/glass sample (B_{WIS}) in Figure S8, right panels]. Possible explanations for this difference would be (i) modification of the chemical structure of the $CsSnBr_3$ samples during transport from WIS to HZB despite being shipped, stored, and handled in inert gas atmosphere or (ii) a spontaneous degradation occurring during the longer time between deposition and characterization (ranging from 2 days to >1 month, see Table S1). The most likely chemical reaction would be the oxidation of (metallic) tin (because of the presence of residual oxygen atoms in the inert gas atmosphere) to a $Sn–O_x$ species, with SnO_2 being the most stable [i.e., Sn would change its oxidation state from 0 (if

metallic tin is inherently present in $CsSnBr_3$) or from +2 (in case that the metallic tin signal detected in the WIS XPS measurements is due to X-ray irradiation) to +4]. Indeed, Sn^{IV} (tin in the oxidation state of +4) derived contributions can be identified in the respective HAXPES shallow core-level spectra. Note that the significantly larger lifetime broadening of the Sn 3d leads to considerable ambiguity in the respective curve fitting results, and thus, we focus on the Sn 4d signal to differentiate between Sn^{II} and Sn^{IV}. In sample A_3, the main and secondary Sn $4d_{5/2}$ fit peak components are found at a binding energy (BE) of (25.6 ± 0.1) and (26.4 ± 0.1) eV, respectively. For sample B_3, they are located at (25.4 ± 0.1) and (26.1 ± 0.1) eV. Hence, for the $CsSnBr_3$ + 20 mol % SnF_2 sample, we find a core-level shift in the range of ($−0.2$ to $−0.3$) eV. Based on the BE positions, we attribute the main and secondary spectral contributions to the Sn 4d spectra to Sn^{II} (tin in the oxidation state of +2) and Sn^{IV},[27] that is, Sn as in $CsSnBr_3$ and a Sn component that is oxidized, relative to $CsSnBr_3$ (e.g., SnO_2). Note that $SnBr_4$, if present, would also contribute to the Sn 4d Sn^{IV} component. The average HAXPES-derived Sn^{II}/Sn^{IV} ratio increases from 1.8 ± 0.5 (for samples without SnF_2 additive) to 3.1 ± 1.6 (see Table 1); that is, the oxidation of Sn is suppressed when SnF_2 is added to the precursor solution.

For A_3 and B_3, the O 2s signal (see Figure 2) at (21.8 ± 0.1) and (21.4 ± 0.1) eV can be attributed to oxygen from (primarily) the TiO_2 substrate as it mainly scales with the intensity of the Ti-related shallow core levels. The near-vanishing of the O 2s signal corroborates the increased coverage of the TiO_2 substrate when SnF_2 is added to the precursor solution (see discussion in conjunction with Figure 1). Note that the observed changes in the O 2s signal can, to some extent, also be ascribed to an increased presence of SnO_2-type Sn^{IV} for the SnF_2-free $CsSnBr_3$ sample as suggested above. Because Sn^{IV}-derived states will act as deep defects in $CsSnBr_3$, a Sn^{IV}-related O 2s signal could, in that respect, also be considered as an indirect probe for the presence of defects.

The peaks at (23.2 ± 0.1) and (23.3 ± 0.1) eV belong to the Cs 5s states.[28] Relative to the respective Sn 4d line intensity, the Cs 5s intensity of sample B_3 is significantly decreased compared to that of sample A_3, indicating a lower Cs/Sn ratio when SnF_2 is added to the precursor solution; the decrease exceeds the expected impact of the additional Sn from the 20 mol % SnF_2 added to the precursor solution of B_3 (see Table 1 and discussion below).

Figure 3 shows the Br 3d spectra of samples A_3 and B_3, including curve fit results. As for the Sn 4d spectra above, the

Table 1. Average Compositions Calculated from the HAXPES Data Shown in Figures 2–4 and in Figures S4–S6 of $CsSnBr_3$ Samples Deposited without (A) and with (B) SnF_2 being Added to the Precursor Solution in Comparison to the Expected Nominal Composition[a]

	Cs/Sn	Br/Sn	F/Sn	Sn(II)/Sn(IV)	Br(m)/Br(s)	Cs(m)/Cs(s)
			Sample(s) A ($CsSnBr_3$)			
nominal	1.00	3.00	N/A	N/A	N/A	N/A
HAXPES	0.5 ± 0.2	2.0 ± 0.6	N/A	1.8 ± 0.5	1.8 ± 0.2	2.8 ± 0.9
			Sample(s) B ($CsSnBr_3$ + 20 mol % SnF_2)			
nominal	0.83	2.50	0.33	N/A	N/A	N/A
HAXPES	0.3 ± 0.1	1.3 ± 0.1	$0.2^b \pm 0.1$	3.1 ± 1.6	4.0 ± 1.4	22.6 ± 24.5

[a]The ratios represent the average of the derived compositions of sample sets $A_{1,3,5}$ and $B_{1,3,5}$, and the stated error margins represent the standard deviation from the average. The Cs/Sn, Br/Sn, and F/Sn ratios are derived considering the total intensity (i.e., main + secondary contribution) of the respective photoemission lines. [b]Obtained from laboratory XPS data.
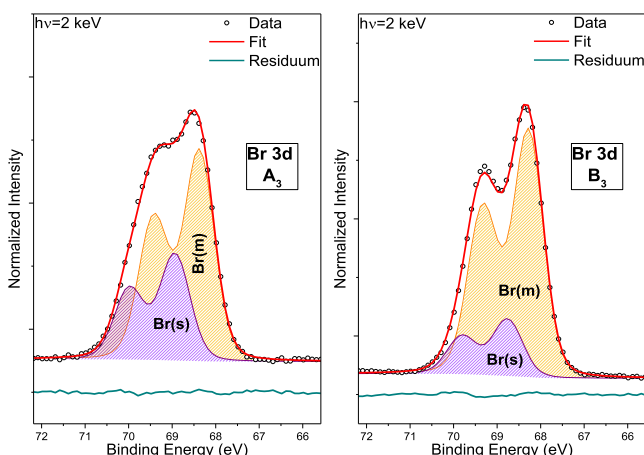
Figure 3. HAXPES detail spectra of the Br 3d energy region of $CsSnBr_3$ (A_3, left panel) and $CsSnBr_3$ + 20 mol % SnF_2 (B_3, right panel), shown with curve fit results. The spectra were normalized by the background intensity at BEs around E_F.

Figure 4. HAXPES Cs 4d detail spectra of $CsSnBr_3$ (A_3, left panel) and $CsSnBr_3$ + 20 mol % SnF_2 (B_3, right panel), shown with curve fit results. The spectra were normalized by the background intensity at BEs around E_F.

satisfactory fits of the Br 3d spectra are only obtained when employing (at least) two peak doublets, indicating the presence of (at least) two different bromine species. The main (m) Br $3d_{5/2}$ fit peak component has a BE of (68.4 ± 0.1) eV for A_3 and (68.3 ± 0.1) eV for B_3 and is ascribed to the chemical bond environment of bromide in $CsSnBr_3$. The secondary (s) peak component in the Br $3d_{5/2}$ fit has a BE of (68.9 ± 0.1) eV for A_3 and (68.8 ± 0.1) eV for B_3 and is attributed to Br–Sn oxide and/or Br–O bonds.[28,29] Comparable to the Sn 4d spectra, we also find a core-level shift of -0.1 eV for the $CsSnBr_3$ + 20 mol % SnF_2 sample.

Accompanying XPS measurements on $CsSnBr_3$ performed at WIS indicate a significantly lower amount of Br(s) (see Figure S5, bottom panel) compared to the Br 3d spectra shown in Figure S5 (upper panels) and Figure 3. However, note that the spectra of $CsSnBr_3$ + 20 mol % SnF_2 samples B_1 and B_{WIS} do show a comparable amount of the secondary bromine species. The fact that we find, however, a significantly different Br(s) contribution of related samples A_1 and A_{WIS} again suggest that transport/storage conditions affect the sample properties. However, some compositional variation in-between deposition runs and/or in a potential SnF_2-related stabilizing effect could also be a reason. Another reason for the varying observations could be the different "probing depth" of the HAXPES and XPS measurements in the case of a pronounced primary/secondary species composition profile in the surface region.

The Cs 4d spectra in Figure 4 also indicate the presence of at least two Cs species. In this case, however, the secondary species appear at lower BE than the main species. The main Cs $4d_{5/2}$ fit peak (i.e., orange area) $[(CsSnBr_3)$ and $(CsSnBr_3$ + 20 mol % $SnF_2)]$ is located at a BE of (75.5 ± 0.1) eV for sample A_3 and (75.4 ± 0.1) eV for B_3; we assume that this main contribution is, similar to the Sn and Br main peaks, associated with a $CsSnBr_3$ chemical environment.[28] The Cs $4d_{5/2}$ fit peak component of the secondary contribution (i.e., purple area) is found at a BE of (74.9 ± 0.1) eV for A_3 and B_3. Attributing the secondary Cs species to an "oxide" species (as was done for Sn and Br) is not straightforward, as Cs oxide-related Cs 4d lines are generally reported (and expected) to be at higher BE values[28] (w.r.t. the main Cs contribution). Careful dosing experiments of metallic Cs with oxygen show that the Cs core levels shift to lower BE values even compared to the Cs lines of
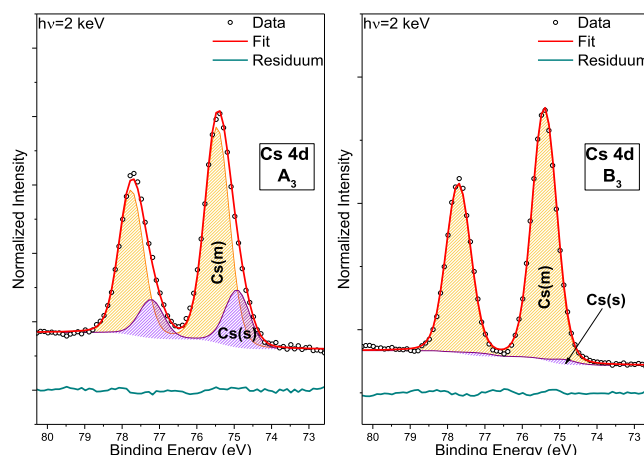
metallic Cs.[30,31] Thus, we speculate that the secondary contribution to the Cs 4d line in our study is also related to a chemical environment best described by Cs "oxide" (see also discussion in conjunction with Figures S6 and S7).

Based on Figures 2–4, a correlation can be drawn between the addition of SnF_2 to the precursor solution and the formation of secondary (oxidized) Sn, Br, and Cs species in Sn-based HaP thin films: the presence of SnF_2 (20 mol %) in the precursor solution seems to generally prevent the formation of (oxidized) secondary phases. This is most obvious from the calculated mean Sn(II)/Sn(IV), Br(m)/Br(s), and Cs(m)/Cs(s) ratios derived from the HAXPES measurements, see Table 1, and supported by the additional data sets $A_{1,5}$ and $B_{1,5}$ (Figures S4–S6). The only exception is the chemical environment of Sn for sample set 5 (see Figure S4), which may be related to it having the lowest F (and thus presumably insufficient SnF_2) content, hypothetically opening a route for additional oxidation of the sample during transport. Moreover, the Cs content for sample B_5 is comparably low (see Table S1).

The observed decrease of Sn^{IV} due to the addition of SnF_2 to the precursor solution has also been observed by Koh et al.[22] Using XPS, they found that much less Sn^{IV} is formed (at the $FASnI_3$ surface) if the precursor solution contained SnF_2 compared to the case where no SnF_2 was added to the precursor solution. At the same time, they reported an enhanced PCE for a solar cell based on the HaP that was prepared from a precursor solution that contained 20 mol % SnF_2.[22] The oxidation of Sn (and its prevention) is of central importance for Sn-based HaPs since the presence of Sn^{IV} will create deep defects that may act as charge carrier recombination centers,[32] which, because of the resulting increase in doping density, will decrease the space charge layer width. If the doping is high enough, this will hinder charge separation. Both effects (creation of deep defects and decreasing space charge layer width) will limit cell efficiency.

The large performance difference between Sn- and Pb-based HaPs is generally associated with the much easier oxidation of Sn^{II} to Sn^{IV} compared to the oxidation of Pb^{II} to Pb^{IV}. Even under carefully controlled conditions, it is difficult (in particular, for wet-chemical synthesis routes) to completely prevent exposure to oxygen, and probably mainly for this

reason—and in contrast to Pb-based HaPs—some degree of oxidation of Sn-based HaPs is likely to occur during preparation. Thus, it is difficult to completely avoid the presence of Sn^{IV}-related deep defects during the preparation process, but their formation can be significantly suppressed by adding excess Sn^{II} (in the form of SnF_2) during HaP preparation.[22]

From the fits of the HAXPES data in Figures 2−4 and S4−S6, the elemental ratios were calculated by correcting the areas of Sn $4d_{5/2}$, Br $3d_{5/2}$, and Cs $4d_{5/2}$ by the photoionization cross section of the respective photoemission line.[33,34] Table 1 summarizes the averaged HAXPES-derived elemental ratios for sample sets $A_{1,3,5}$ ($CsSnBr_3$) and $B_{1,3,5}$ ($CsSnBr_3$ + 20 mol % SnF_2) and the nominal compound composition, as expected from the reagent concentrations. The ratios for the individual batches and the respective ratios for the accompanying XPS analysis at WIS can be found in the Supporting Information (see Table S1). We observe that for sample sets A and B, the HAXPES-derived compositions significantly deviate from the expected values and that there is also variation between the individual samples within one sample set. However, the smaller standard deviations for the average compositions derived for the samples of $CsSnBr_3$ + 20 mol % SnF_2 than for those without SnF_2 (Table 1) indicate a reduced variation of the experimental data between sample sets upon addition of SnF_2. Most striking in the comparison with the nominal (and assumed bulk) Cs/Sn = 1 (0.83) and Br/Sn = 3 (2.5) compositions expected for $CsSnBr_3$ ($CsSnBr_3$ + 20 mol % SnF_2) samples is the lower Cs/Sn = 0.5 ± 0.2 (0.3 ± 0.1) and Br/Sn = 2.0 ± 0.6 (1.3 ± 0.1) values. Such values reveal an enrichment of tin and a deficiency of cesium in the surface region of the sample (which is enhanced for the $CsSnBr_3$ samples where SnF_2 was added to the precursor solution). The more surface-sensitive XPS Cs/Sn ratios derived at WIS of 0.15 (0.12) and Br/Sn ratios of 1.33 (0.76) (see Table S1 in the Supporting Information) suggest even stronger Sn enrichment and Cs deficiency on the top surface. This is in line with the observation of Marshall et al.,[26] who provide clear evidence of the accumulation of $SnCl_2$ at the surface of $CsSnI_3$ + 10 mol % $SnCl_2$ films. Similarly, the work of Liao et al.[23] suggests the accumulation of SnF_2 at the surface of $FASnI_3$ + 20 mol % SnF_2 samples. This additive accumulation at the surface of perovskite samples is further supported by Kumar et al.,[32] showing that SnF_2 is not integrated into the $CsSnI_3$ lattice structure for any concentration between 5 and 40 mol %.

The addition of SnF_2 to the precursor solution results in the suppression of the secondary Cs and Br species and the Sn^{II} to Sn^{IV} oxidation (see discussion). The variation between batches in each set (see Table S1 in the Supporting Information) shows the importance of this study of reproducibility and can be explained by two main factors: (insufficient) reproducibility of sample preparation and/or sample modification due to environmental and handling effects during packaging/transport/storage. The latter issue becomes apparent when comparing the HAXPES data collected at HZB with the XPS data measured at WIS for sample set A: in the XPS data, a lower presence of the secondary species for Br can be observed for the $CsSnBr_3$ samples (see Table S1 in the Supporting Information), while the opposite is observed for the Cs(m)/Cs(s) (see Table S1). A decreased presence of the oxidized species in the more surface-sensitive XPS data of Br is likely not related to a "depth gradient" in oxidation because exposure to an oxidizing atmosphere would preferentially affect the

surface. Therefore, we ascribe the observed differences to the increased time between preparation and measurement of the samples and/or their transport conditions for the HAXPES experiments compared to the XPS measurements performed at WIS. The addition of SnF_2 to the precursor solution seems to similarly affect the increase of the Br(m)/Br(s) ratio, when comparing the XPS and averaged HAXPES data (ca. a factor of 2, see Tables 1 and S1 in the Supporting Information).

In the following, we can only discuss the derived composition ratios and species that are potentially present, speculating on possible scenarios that are consistent with the HAXPES-derived compositions, rather than giving definitive answers. Considering both, the main and secondary components of the fits, the composition found for sample set A is in general agreement with the presence of $CsSnBr_3$ and varying additional species of, for example, $SnBr_2$ and/or $CsSn_2Br_5$,[35] in (on) the samples (surfaces), which can rationalize the experimentally found Cs deficiency and Sn enrichment. The main difference for sample set B is the decrease of the Cs/Sn and Br/Sn ratios, which is somewhat in agreement with the addition of SnF_2 to the precursor solution; however, the change (i.e., by a factor of ca. 1.5 on average) is higher than expected for an addition of 20 mol % SnF_2 to the precursor solution. Thus, we speculate that the addition of SnF_2 has a disproportionately large effect on the surface of the $CsSnBr_3$ + 20 mol % SnF_2 sample.

An interpretation of the elemental ratios of the secondary Cs and Br species and the Sn^{IV} component is less straightforward, mainly because of the large number of possible Sn^{IV} species [possible candidates are SnO_2, $Sn(BrO_3)_4$, and/or Cs_2SnBr_6] and, thus, we will refrain from doing so.

In order to decide whether the observed chemical structure variations between batches in each sample set is caused by (insufficient) reproducibility of sample preparation or by environmental and handling effects, more controlled in-system experiments (i.e., sample preparation and characterization in one system without intermediate air exposure) will be needed.

In order to shed some light on the underlying mechanism of the observed SnF_2-induced effects on the chemical composition and layer morphology, we note that the quality of Sn-based perovskite films depends on various parameters. A central factor seems to be the ability to minimize the $Sn^{II} \rightarrow Sn^{IV}$ oxidation and the related formation of Sn vacancies. Kumar et al.[32] proposed that SnF_2 addition to the precursor solution results in an increase of the defect formation energy of Sn vacancies in correspondingly prepared $CsSnI_3$ perovskites. Therefore, we speculate that this higher formation energy not only limits the presence of Sn vacancies but also prevents/minimizes the accompanied creation of unwanted secondary species [in our case, the Sn^{IV}, Br(s) and Cs(s) components of the discussed Sn 4d, Br 3d, and Cs 4d shallow core levels], which might also benefit film morphology, that is, improving substrate coverage.

2.1. Effect of SnF₂ on Electronic Structure.
Based on the results of the chemical analysis of (the surface of) the $CsSnBr_3$ and $CsSnBr_3$ + 20 mol % SnF_2 samples, we will now discuss the electronic structure of this absorber class. The HAXPES VB spectra on a linear scale are presented in Figure 5 for samples A_3 and B_3 [see Figure S9 for the individual VB spectra and VB maximum (VBM) determination of all samples and Figure S10 for the VB spectra represented on a semilog scale].
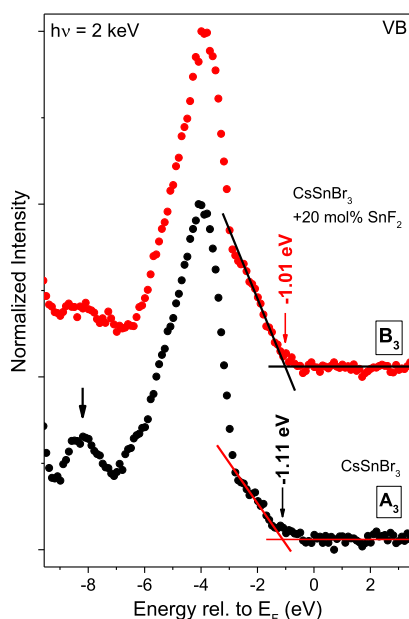
Figure 5. HAXPES spectra of the energy region near the VBM of $CsSnBr_3$ (A$_3$) and $CsSnBr_3$ + 20 mol % SnF$_2$ (B$_3$) samples, including the VBM values (± 0.10 eV) determined by linear extrapolation of the leading edges on a linear scale. A vertical offset is added for clarity.

Theoretical DOS calculations predict that the VB region of $CsSnBr_3$ is dominated by hybridized Br 4p and Sn 5s states,[36] and the measured spectral shape of the VB region is in agreement with the calculated DOS. The VB spectrum of the $CsSnBr_3$ sample has a more pronounced feature at BE ≈ 8 eV (indicated by an arrow in Figure 5 and in the left panel of Figure S9) compared to the spectrum of the $CsSnBr_3$ + 20 mol % SnF$_2$ sample. This feature is ascribed to O 2p-derived DOS originating from the TiO_2 substrate, which is visible due to incomplete coverage (see discussion above).[25]

The feature at BE ≈ 2 eV (indicated by an arrow in the right panel of Figure S9) can be ascribed to states with a strong Sn 5s characteristic, and a DOS increase in this region can be observed in the spectra of the sample for which 20 mol % SnF$_2$ was added to the precursor solution. This change is consistent with the (observed) change in Sn-oxidation state:[27,37] a decrease in relative concentration of Sn^{IV} with respect to Sn^{II} results in a change in nominal electron configuration from $4d^{10}$ $5s^0$ $5p^0$ to $4d^{10}$ $5s^2$ $5p^0$ and, thus, a corresponding increase of electron density in this spectral range.

The VBM values derived by linear extrapolation for samples A$_3$ [(-1.11 ± 0.10) eV] and B$_3$ [(-1.01 ± 0.10) eV] indicate a small shift of the VBM toward E_F when SnF$_2$ is added during deposition, in agreement with ref 12. The averaged VB spectra shown by the thick lines in the right panel of Figure S9 can, however, be scaled so that they appear to overlay each other in the VBM region. Nishikubo et al.[37] also found no VBM change of $MASnI_3$ or $FASnI_3$, independent of adding SnF$_2$ to the precursor solution. Based on the measurements shown here, the disappearance or overshadowing of the small (average) VBM shift can, however, certainly be attributed to the differing, mixed chemical surface compositions discussed above. Previously, the VBM positions of −1.7 and −1.6 eV[19] for similarly prepared $CsSnBr_3$ and $CsSnBr_3$ + 20 mol % SnF$_2$ samples, respectively, have been reported. As these values have been derived by ultraviolet photoelectron spectroscopy (UPS,

He I = 21.2 and He II = 40.8 eV), the discrepancy to the more bulk-sensitive HAXPES (2 keV)-derived values of −1.11 and −1.01 (± 0.10) eV can be explained by an increased impact of surface contaminants on the VBM determination and/or a pronounced downward band bending (assuming p-type bulk conductivity) toward the sample surface (see discussion below). In addition, a certain impact of a low-excitation energy-induced k-selectivity of the photoemission process cannot be excluded. Furthermore, it has to be considered that the top of the $CsSnBr_3$ VB is formed by Sn 5s-derived states,[36] to which HAXPES measurements are more sensitive than UPS measurements (see the Supporting Information discussion related to Figure S10 for details). Thus, the seemingly high UPS-derived VBM values—also compared to the band gap of $CsSnBr_3$: 1.75 eV[19]—could be explained by the spectral onset that is (at this excitation energy) dominated by Br 4p-derived states. The thus presumably overshadowed "real" onset formed by Sn 5s-derived states might mistakenly be interpreted as a background when doing the linear approximation of the leading edge. A solution for this issue could be the presentation and evaluation of the VB spectra on a semilogarithmic scale as suggested by Endres et al.[38] The direct comparison of the HAXPES VBM values determined by linear approximation of the leading edge on a linear scale and the respective spectra shown on a semilogarithmic scale are shown in Figure S10. As the HAXPES spectra do have a significantly higher noise level above the VBM than the UPS data (inherent to the experimental setup, see the Supporting Information for more details), it is not straightforward to use the semilogarithmic HAXPES plots to derive VBM positions without respective DOS calculations. However, the VBM values derived on a linear scale mainly coincide within the experimental uncertainty with the clear intensity drop of the semilogarithmic HAXPES data, and thus, we conclude that in the case of HAXPES for this Sn-based HaP, a semilog approach does not lead to significantly different VBM values. Reasons for that could be the relatively high photoionization cross section for s-derived states when employing hard X-rays (instead of UV light, see discussion above) and the higher DOS at the top of the VB of $CsSnBr_3$ compared to that of $CsPbBr_3$,[39] for which the benefit of the semilog approach was demonstrated.[38]

Taking the $CsSnBr_3$ bulk band gap of 1.75 eV (as derived by UV−Vis spectrophotometry for similarly prepared samples[19]) into account, the HAXPES-derived VBM positions may be interpreted in terms of two scenarios. Assuming that there is no (depth-dependent) chemical and electronic structure profile (i.e., somewhat neglecting the finding of a Sn-rich and Cs-/Br-poor $CsSnBr_3$ surface), the VBMs (independent of SnF$_2$) indicate a very slight n-type (bulk) conductivity. Assuming p-type conductivity in the bulk, the derived VBM positions are in agreement with a conduction-type inversion at the surface (for a p-type semiconductor, one would expect |VBM| < |CBM| = E_g − |VBM|, with CBM being the conduction band minimum), most likely due to a high density of acceptor-like surface states, causing a significant (downward) surface band bending.

By focusing on each sample set (A$_n$, B$_n$) individually, we find that in two (n: 3 and 5) of the three cases, we can observe a SnF$_2$-induced shift of the VBM toward E_F. The VBM (A$_5$)− VBM (B$_5$) shift of −0.18 eV (± 0.14 eV) represents the upper boundary in our case. In the first scenario (i.e., n-type bulk conductivity), this shift indicates a decrease in the net n-type doping concentration. For the second scenario (i.e., p-type

bulk conductivity), the VBM shift toward E_F would indicate a reduced downward surface band bending, for example, due to a reduced density of acceptor-like defect (surface) states and/or an increased p-type doping in the material bulk.

E_F being closer to the CBM than to the VBM, as well as the VBM shift, are—within experimental uncertainty—in agreement with previous UPS measurements[19] (see discussion above) and with the core-level shifts discussed above. The fact that the VBM values derived by the more surface-sensitive UPS[19] are farther from E_F than in the HAXPES measurements, supporting the second scenario (i.e., p-type bulk conductivity and downward surface band bending).

We have previously shown how oxidation of Sn^{II} to Sn^{IV} in $CsSnBr_3$ can result in p-type doping.[12] Other studies have also shown that inhibiting Sn-oxidation by using SnF_2 in the preparation leads to a reduction of the hole concentration in Sn-based HaPs by 1−2 orders of magnitude.[23,24,32] Thus, in a simple picture, preventing this oxidation (by addition of SnF_2) should result in a shift of the VBM away from E_F, contrary to what we observe. Apparently, the SnF_2-induced VBM shift toward E_F is mainly governed by the increase in Sn 5s-derived DOS as a result of the change in Sn-oxidation state (i.e., the decrease of Sn^{IV}-derived defects) and corresponding electron configuration modification (see discussion above). However, assuming p-type bulk conductivity, one could also speculate that the VBM shift toward E_F may to some extent be due to a SnF_2 addition-induced reduction of the density of (acceptor-like) defect states at the surface, resulting in a less pronounced surface band bending. This conclusion is supported by refs 24 and 32 that correlate SnF_2 with the reduction of the density of (interband) defect states.

It has been reported[26] that any excess of Sn^{II} (from SnX_2 additives, X = Cl, Br, and I) can result in an improved device performance, yet addition of excess $SnBr_2$ during $CsSnBr_3$ preparation has only a very small effect on performance compared to the improvement when using SnF_2.[20] Thus, on the one hand, the incorporation of excess Sn and its effect/benefits to the film properties can be specific to the individual perovskite; on the other hand, one could speculate that the results of this study w.r.t. the observed SnF_2 addition-induced chemical and electronic structure changes can, to some extent, also be transferred to these systems. However, detailed studies are required to conclusively answer this question.

3. CONCLUSIONS

The chemical and electronic structure of $CsSnBr_3$ thin-film solar cell absorbers and how it is impacted by the addition of 20 mol % SnF_2 to the precursor solution has been studied by lab-based soft (XPS) and synchrotron-based hard (HAXPES) X-ray photoelectron spectroscopy. To determine the reproducibility and reliability of the results, several of (nominally identically prepared) sample sets were investigated. Variations in the HAXPES-derived surface compositions between individual sample sets were observed. Despite such variability, we find that the addition of 20 mol % SnF_2 results in an improved coverage of the TiO_2 substrate by $CsSnBr_3$, in agreement with earlier reports, a decrease in the oxidation of Sn^{II} to Sn^{IV}, and a suppression in the formation of secondary Br and Cs species. Comparing HAXPES-derived compositions with the nominal compositions reveals an overall enrichment in tin and deficiency of cesium in the surface region, which is further enhanced by the addition of SnF_2 to the precursor solution. The HAXPES VB spectra show a SnF_2-induced

redistribution of Sn 5s-derived DOS, reflecting the changing Sn^{II}/Sn^{IV} ratio. Furthermore, we suggest—despite some variation between sample batches—a VBM shift toward E_F upon SnF_2 addition to the precursor solution. This can be explained by a reduction of the density of acceptor-like (surface) defects, which results in a less pronounced surface band bending. Finally, the improvement of the performance of $CsSnBr_3$-based solar cells, prepared with SnF_2, can likely be related to the reduction of Sn^{IV}-derived states, decreasing the density of deep defects in the $CsSnBr_3$ perovskite absorber (thus, effectively reducing the number of charge carrier recombination centers) and maintaining a moderate doping density that will result in a suitable space charge layer width (thus, maintaining sufficient charge separation).

■ ASSOCIATED CONTENT

ⓈⒾ Supporting Information

The Supporting Information is available free of charge at https://pubs.acs.org/doi/10.1021/acsami.9b22967.

> Data analysis and description of the XPS and HAXPES spectra; complete set of shallow (Cs 4d, Br 3d, and Sn 4d) core-level HAXPES spectra as well as F 1s XPS, Cs 3d and Sn 3d HAXPES, and XPS; Br 3d XPS spectra; and table of elemental ratios as well as VB spectra for all samples (PDF)

■ AUTHOR INFORMATION

Corresponding Authors

Gary Hodes − *Department of Materials & Interfaces, Weizmann Institute of Science (WIS), 7610001 Rehovot, Israel;* ⓞ orcid.org/0000-0001-7798-195X; Email: gary.hodes@weizmann.ac.il

David Cahen − *Department of Materials & Interfaces, Weizmann Institute of Science (WIS), 7610001 Rehovot, Israel;* ⓞ orcid.org/0000-0001-8118-5446; Email: david.cahen@weizmann.ac.il

Marcus Bär − *Interface Design, Energy Materials In-Situ Laboratory Berlin (EMIL), and Helmholtz-Institute Erlangen-Nürnberg for Renewable Energy (HI ERN), Helmholtz-Zentrum Berlin für Materialien und Energie GmbH (HZB), 14109 Berlin, Germany; Department of Chemistry & Pharmacy, Friedrich-Alexander-Universität Erlangen-Nürnberg, 91058 Erlangen, Germany;* ⓞ orcid.org/0000-0001-8581-0691; Email: marcus.baer@helmholtz-berlin.de

Authors

Claudia Hartmann − *Interface Design, Helmholtz-Zentrum Berlin für Materialien und Energie GmbH (HZB), 14109 Berlin, Germany;* ⓞ orcid.org/0000-0002-8017-8161

Satyajit Gupta − *Department of Materials & Interfaces, Weizmann Institute of Science (WIS), 7610001 Rehovot, Israel; Department of Chemistry, Indian Institute of Technology Bhilai, Chhattisgarh 492015, India*

Tatyana Bendikov − *Chemical Research Support Unit, Weizmann Institute of Science (WIS), Rehovot 7610001, Israel*

Xeniya Kozina − *Interface Design, Helmholtz-Zentrum Berlin für Materialien und Energie GmbH (HZB), 14109 Berlin, Germany*

Thomas Kunze − *Interface Design, Helmholtz-Zentrum Berlin für Materialien und Energie GmbH (HZB), 14109 Berlin, Germany*

Roberto Félix − *Interface Design, Helmholtz-Zentrum Berlin für Materialien und Energie GmbH (HZB), 14109 Berlin, Germany;* ⊙ orcid.org/0000-0002-3620-9899

Regan G. Wilks − *Interface Design and Energy Materials In-Situ Laboratory Berlin (EMIL), Helmholtz-Zentrum Berlin für Materialien und Energie GmbH (HZB), 14109 Berlin, Germany*

Complete contact information is available at:
https://pubs.acs.org/10.1021/acsami.9b22967

Author Contributions

C.H. and S.G. contributed equally to this work. The manuscript was written through contributions from all authors. All authors have given approval to the final version of the manuscript.

Notes

The authors declare no competing financial interest.

■ REFERENCES

(1) Park, N.-G.; Grätzel, M.; Miyasaka, T.; Zhu, K.; Emery, K. Towards Stable and Commercially Available Perovskite Solar Cells. *Nat. Energy* **2016**, *1*, 16152.

(2) Mehmood, U.; Al-Ahmed, A.; Afzaal, M.; Al-Sulaiman, F. A.; Daud, M. Recent Progress and Remaining Challenges in Organometallic Halides Based Perovskite Solar Cells. *Renewable Sustainable Energy Rev.* **2017**, *78*, 1−14.

(3) Asghar, M. I.; Zhang, J.; Wang, H.; Lund, P. D. Device Stability of Perovskite Solar Cells − A Review. *Renewable Sustainable Energy Rev.* **2017**, *77*, 131−146.

(4) www.nrel.gov/pv/assets/images/efficiency-chart.png (accessed 2020-02-28).

(5) Giustino, F.; Snaith, H. J. Toward Lead-Free Perovskite Solar Cells. *ACS Energy Lett.* **2016**, *1*, 1233−1240.

(6) Konstantakou, M.; Stergiopoulos, T. Critical Review on Tin Halide Perovskite Solar Cells. *J. Mater. Chem. A* **2017**, *5*, 11518−11549.

(7) Toshniwal, A.; Kheraj, V. Development of Organic-Inorganic Tin Halide Perovskites: A Review. *Sol. Energy* **2017**, *149*, 54−59.

(8) Stoumpos, C. C.; Frazer, L.; Clark, D. J.; Kim, Y. S.; Rhim, S. H.; Freeman, A. J.; Ketterson, J. B.; Jang, J. I.; Kanatzidis, M. G. Hybrid Germanium Iodide Perovskite Semiconductors: Active Lone Pairs, Structural Distortions, Direct and Indirect Energy Gaps, and Strong Nonlinear Optical Properties. *J. Am. Chem. Soc.* **2015**, *137*, 6804−6819.

(9) McClure, E. T.; Ball, M. R.; Windl, W.; Woodward, P. M. Cs_2AgBiX_6 (X = Br, Cl): New Visible Light Absorbing, Lead-Free Halide Double Perovskite Semiconductors. *Chem. Mater.* **2016**, *28*, 1348−1354.

(10) Filip, M. R.; Hillman, S.; Haghighirad, A. A.; Snaith, H. J.; Giustino, F. Band Gaps of the Lead-Free Halide Double Perovskites $Cs_2BiAgCl_6$ and $Cs_2BiAgBr_6$ from Theory and Experiment. *J. Phys. Chem. Lett.* **2016**, *7*, 2579−2585.

(11) Slavney, A. H.; Hu, T.; Lindenberg, A. M.; Karunadasa, H. I. A Bismuth-Halide Double Perovskite with Long Carrier Recombination Lifetime for Photovoltaic Applications. *J. Am. Chem. Soc.* **2016**, *138*, 2138−2141.

(12) Gupta, S.; Cahen, D.; Hodes, G. How SnF_2 Impacts the Material Properties of Lead-Free Tin Perovskite. *J. Phys. Chem. C* **2018**, *122*, 13926−13936.

(13) Ke, W.; Stoumpos, C. C.; Kanatzidis, M. G. "Unleaded" Perovskites: Status Quo and Future Prospects of Tin-Based Perovskite Solar Cells. *Adv. Mater.* **2019**, *31*, 1803230.

(14) Hao, F.; Stoumpos, C. C.; Cao, D. H.; Chang, R. P. H.; Kanatzidis, M. G. Lead-Free Solid-State Organic−Inorganic Halide Perovskite Solar Cells. *Nat. Photonics* **2014**, *8*, 489−494.

(15) Shockley, W.; Queisser, H. J. Detailed Balance Limit of Efficiency of p-n Junction Solar Cells. *J. Appl. Phys.* **1961**, *32*, 510−519.

(16) Jokar, E.; Chien, C.-H.; Tsai, C.-M.; Fathi, A.; Diau, E. W.-G. Robust Tin-Based Perovskite Solar Cells with Hybrid Organic Cations to Attain Efficiency Approaching 10%. *Adv. Mater.* **2019**, *31*, 1804835.

(17) Gorgoi, M.; Svensson, S.; Schäfers, F.; Öhrwall, G.; Mertin, M.; Bressler, P.; Karis, O.; Siegbahn, H.; Sandell, A.; Rensmo, H.; Doherty, W.; Jung, C.; Braun, W.; Eberhardt, W. The High Kinetic Energy Photoelectron Spectroscopy Facility at BESSY Progress and First Results. *Nucl. Instrum. Methods Phys. Res., Sect. A* **2009**, *601*, 48−53.

(18) Schaefers, F.; Mertin, M.; Gorgoi, M. KMC-1: A High Resolution and High Flux Soft X-ray Beamline at BESSY. *Rev. Sci. Instrum.* **2007**, *78*, 123102.

(19) Gupta, S.; Bendikov, T.; Hodes, G.; Cahen, D. $CsSnBr_3$, A Lead-Free Halide Perovskite for Long-Term Solar Cell Application: Insights on SnF_2 Addition. *ACS Energy Lett.* **2016**, *1*, 1028−1033.

(20) Gupta, S.; Hodes, G. Effect of SnF_2 Concentration on the Optoelectronic and PV Cell Properties of $CsSnBr_3$. *SN Appl. Sci.* **2019**, *1*, 1066.

(21) Tougaard, S. *QUASES-IMFP-TPP2M*; Quases-Tougaard Inc., 2002.

(22) Koh, T. M.; Krishnamoorthy, T.; Yantara, N.; Shi, C.; Leong, W. L.; Boix, P. P.; Grimsdale, A. C.; Mhaisalkar, S. G.; Mathews, N. Formamidinium Tin-based Perovskite with Low Eg for Photovoltaic Applications. *J. Mater. Chem. A* **2015**, *3*, 14996−15000.

(23) Liao, W.; Zhao, D.; Yu, Y.; Grice, C. R.; Wang, C.; Cimaroli, A. J.; Schulz, P.; Meng, W.; Zhu, K.; Xiong, R.-G.; Yan, Y. Lead-Free Inverted Planar Formamidinium Tin Triiodide Perovskite Solar Cells Achieving Power Conversion Efficiencies up to 6.22%. *Adv. Mater.* **2016**, *28*, 9333−9340.

(24) Xing, G.; Kumar, M. H.; Chong, W. K.; Liu, X.; Cai, Y.; Ding, H.; Asta, M.; Grätzel, M.; Mhaisalkar, S.; Mathews, N.; Sum, T. C. Solution-Processed Tin-Based Perovskite for Near-Infrared Lasing. *Adv. Mater.* **2016**, *28*, 8191−8196.

(25) Liao, Y.; Liu, H.; Zhou, W.; Yang, D.; Shang, Y.; Shi, Z.; Li, B.; Jiang, X.; Zhang, L.; Quan, L. N.; Quintero-Bermudez, R.; Sutherland, B. R.; Mi, Q.; Sargent, E. H.; Ning, Z. Highly Oriented Low-Dimensional Tin Halide Perovskites with Enhanced Stability and Photovoltaic Performance. *J. Am. Chem. Soc.* **2017**, *139*, 6693−6699.

(26) Marshall, K. P.; Walker, M.; Walton, R. I.; Hatton, R. A. Enhanced Stability and Efficiency in Hole-Transport-Layer-Free $CsSnI_3$ Perovskite Photovoltaics. *Nat. Energy* **2016**, *1*, 16178.

(27) De Padova, P.; Fanfoni, M.; Larciprete, R.; Mangiantini, M.; Priori, S.; Perfetti, P. A Synchrotron Radiation Photoemission Study of the Oxidation of Tin. *Surf. Sci.* **1994**, *313*, 379−391.

(28) National Institute of Standards and Technology. NIST X-ray Photoelectron Spectroscopy (XPS) Database [Online], available http://srdata.nist.gov/xps/Default.aspx (accessed 2020-02-03).

(29) Jung, M.-C.; Raga, S. R.; Qi, Y. Properties and Solar Cell Applications of Pb-Free Perovskite Films Formed by Vapor Deposition. *RSC Adv.* **2016**, *6*, 2819−2825.

(30) Spicer, W. E.; Lindau, I.; Su, C. Y.; Chye, P. W.; Pianetta, P. Core-level Photoemission of the Cs-O Adlayer of NEA GaAs Cathodes. *Appl. Phys. Lett.* **1978**, *33*, 934−935.

(31) Hrbek, J.; Yang, Y. W.; Rodriguez, J. A. Oxidation of Cesium Multilayers. *Surf. Sci.* **1993**, *296*, 164−170.

(32) Kumar, M. H.; Dharani, S.; Leong, W. L.; Boix, P. P.; Prabhakar, R. R.; Baikie, T.; Shi, C.; Ding, H.; Ramesh, R.; Asta, M.; Graetzel, M.; Mhaisalkar, S. G.; Mathews, N. Lead-Free Halide Perovskite Solar Cells with High Photocurrents Realized Through Vacancy Modulation. *Adv. Mater.* **2014**, *26*, 7122−7127.

(33) Trzhaskovskaya, M. B.; Nefedov, V. I.; Yarzhemsky, V. G. Photoelectron Angular Distribution Parameters for Elements Z=1 to Z=54 in the Photoelectron Energy Range 100−5000 eV. *At. Data Nucl. Data Tables* **2001**, *77*, 97−159.

(34) Trzhaskovskaya, M. B.; Nefedov, V. I.; Yarzhemsky, V. G. Photoelectron Angular Distribution Parameters for Elements Z=55 to Z=100 in the Photoelectron Energy Range 100−5000 eV. *At. Data Nucl. Data Tables* **2002**, *82*, 257−311.

(35) Sabba, D.; Mulmudi, H. K.; Prabhakar, R. R.; Krishnamoorthy, T.; Baikie, T.; Boix, P. P.; Mhaisalkar, S.; Mathews, N. Impact of Anionic Br− Substitution on Open Circuit Voltage in Lead Free Perovskite ($CsSnI_{3-x}Br_x$) Solar Cells. *J. Phys. Chem. C* **2015**, *119*, 1763−1767.

(36) Zheng, J.-C.; Huan, C. H. A.; Wee, A. T. S.; Kuok, M. H. Electronic Properties of $CsSnBr_3$: Studies by Experiment and Theory. *Surf. Interface Anal.* **1999**, *28*, 81−83.

(37) Nishikubo, R.; Ishida, N.; Katsuki, Y.; Wakamiya, A.; Saeki, A. Minute-Scale Degradation and Shift of Valence-Band Maxima of $(CH_3NH_3)SnI_3$ and $HC(NH_2)_2SnI_3$ Perovskites upon Air Exposure. *J. Phys. Chem. C* **2017**, *121*, 19650−19656.

(38) Endres, J.; Egger, D. A.; Kulbak, M.; Kerner, R. A.; Zhao, L.; Silver, S. H.; Hodes, G.; Rand, B. P.; Cahen, D.; Kronik, L.; Kahn, A. Valence and Conduction Band Densities of States of Metal Halide Perovskites: A Combined Experimental−Theoretical Study. *J. Phys. Chem. Lett.* **2016**, *7*, 2722−2729.

(39) Mao, X.; Sun, L.; Wu, T.; Chu, T.; Deng, W.; Han, K. First-Principles Screening of All-Inorganic Lead-Free ABX3 Perovskites. *J. Phys. Chem. C* **2018**, *122*, 7670−7675.